ISSN 1027-5495. Functional Materials, 33, No.3 (2026), p. 492-501
doi:http://dx.doi.org/10.15407/fm33.03.492 © 2026 — SSI "Institute for Single Crystals"
This is an open access article under the CC BY-NC-ND license (http://creativecommons.org/licenses/by-nc-nd/4.0/).

Microstructure, magnetic and electric properties of ground and sintered powder mixture 20.0 wt% Fe and 80.0 wt% $BaTiO_3$

Milica Spasojevic Savkovic[1] , Milentije Lukovic [2*],
Aleksa Maricic[2], Miroslav Spasojevic[2]

[1] Innovative Centre of the Faculty of Chemistry, Studentski trg 1, 2-16 Belgrade, University of Belgrade, Serbia
[2] Joint laboratory for Advanced Materials of SASA, Section for Amorphous Systems, Faculty of Technical Sciences, Svetog save 65 Čačak, Serbia
*corresponding author: milentije.lukovic@ftn.kg.ac.rs

Received January 14, 2026, approved July 25, 2026

The effect of grinding and sintering of a powder mixture containing 20.0 wt% Fe and 80.0 wt% $BaTiO_3$ on the morphology, chemical composition, microstructure, as well as magnetic and electric properties of the obtained samples was investigated. The sintered samples consisted of plate-like grains with sizes ranging from 0.3 to 4.2 μm. Grinding the powder for up to 90 min resulted in samples composed of a matrix containing crystalline BaTiO3 together with the amorphous $BaTiO_3$ and TiO_2 phases, in which $BaFe_{12}O_{19}$ and $Ba_{1.696}Ti_{0.228}O_3$ crystallites were embedded. In the samples ground for more than 90 min, $BaTiO_3$ became completely amorphous. The magnetization increased with grinding time up to 90 min and then gradually declined. The magnetization remained nearly constant upon heating to 100 °C, decreased between 100 and 250 °C and remained essentially unchanged from 250 °C to 470 °C. Above 470 °C, the magnetization decreased progressively until the Curie temperature was reached. The relative electric permittivity increased with increasing grinding time and decreased with increasing frequency.

Keywords: grinding; sintering; barium titanate; barium hexaferrite; multiferroic; magnetic and electric properties

Мікроструктура, магнітні та електричні властивості помеленої та спеченої порошкової суміші 20,0 мас.% Fe та 80,0 мас.% $BaTiO_3$ *Milica Spasojevic Savkovic, Milentije Lukovic, Aleksa Maricic, Miroslav Spasojevic* [4]

Досліджено вплив подрібнення та спікання порошкової суміші, що містить 20,0 мас.% Fe та 80,0 мас.% $BaTiO_3$, на морфологію, хімічний склад, мікроструктуру, магнітні та електричні властивості отриманих зразків. Спечені зразки містили пластинчасті зерна розміром від 0,3 до 4,2 мкм. В результаті подрібнення порошку протягом до 90 хвилин були отримані зразки, що складаються з матриці, що містить кристалічний $BaTiO_3$ разом з аморфними фазами $BaTiO_3$ і TiO_2, які містять кристаліти $BaFe_{12}O_{19}$ і $Ba_{1,696}Ti_{0,228}O_3$. У зразках, подрібнених понад 90 хвилин, $BaTiO_3$ став повністю аморфним. Намагніченість зростала зі збільшенням часу шліфування до 90 хвилин, та поступово знижувалася. Намагніченість залишалася практично постійною при нагріванні до 100°C, зменшувалася між 100 і 250°C і практично не змінювалася від 250°C до 470°C. При температурі вище 470 °C намагніченість поступово зменшувалася, доки не було досягнуто температури Кюрі. Відносна електрична проникність збільшується із збільшенням часу шліфування та зменшується із збільшенням частоти.

1. Introduction

Multiferroic materials are unique since they exhibit two or more ferroic order parameters simultaneously. Owing to the coexistence of electrical and magnetic ordering, these materials have attracted considerable attention for a wide range of technological applications, including microelectronic devices, such as microwave phase shifters, magnetically controlled electro-optic devices and broadband magnetic sensors [1-6]. However, the simultaneous realization of ferroelectricity and magnetism in a single-phase material remains challenging due to the intrinsic incompatibility of the mechanisms responsible for these properties as well as difficulties associated with their synthesis. Consequently, two-phase composite ceramics have been developed as an alternative class of multiferroics with enhanced magnetic and electric properties [7, 8]. In such materials, the coupling between the ferroelectric and ferromagnetic phases allows for the control of electric polarization by an applied magnetic field and the tuning of magnetic properties by an applied electric field [9].

$BaTiO_3$ is one of the most extensively studied ferroelectric ceramics with a wide range of applications, including multilayer ceramic capacitors and piezoelectric devices such as underwater transducers [7-19]. However, for practical application, ferroelectric ceramics must exhibit a high dielectric constant together with adequate resistivity properties in small volumes. Substantial improvements in dielectric performance of $BaTiO_3$-based ceramics have been achieved through modification with various titanate compounds [3, 14, 17, 18].

Multiferroic composites can be fabricated by combining a ferroelectric phase, such as $BaTiO_3$, with a ferromagnetic material or its oxide, thereby integrating the desirable properties of both constituents into a single material system [11, 15-40].

In the present study, a multiferroic composite consisting of $BaTiO_3$ as a ferroelectric matrix and $BaFe_{12}O_{19}$ as a magnetic secondary phase was synthetsized and characterized. Barium hexaferrite, $BaFe_{12}O_{19}$ is a permanent magnet widely used in electronic and microwave devices because of its high coercivity, excellent chemical stability, corrosion and moisture resistance and low production cost [11-13, 41-48]. Various synthesis routes have been employed to prepare $BaFe_{12}O_{19}$ powders, including coprecipitation, sol-gel combustion, micro-emulsion, electrodeposition and ball milling [12, 13, 34, 41-52]. The synthesis method has a substantial influence on the characteristics, such as the microstructure morphology, and the electrical and magnetic properties of $BaFe_{12}O_{19}$ [33, 34, 41, 44, 47-56]. In particular, mechanochemical activation by grinding enhances the rate of $BaFe_{12}O_{19}$ formation since the particle size reduction increases the specific surface area and promotes the contact between the reactants [16, 30, 31, 33, 34]. Consequently, the grinding time strongly affects the kinetics of phase formation, allowing the sintering temperature and duration to be reduced or optimized [16, 33, 34, 44]. Furthermore, grinding time affects the morphology and microstructure of the obtained powders, which in turn determine their electrical and magnetic properties [33, 34, 44]. Previous studies on mechanochemically synthesized $BaFe_{12}O_{19}$ have shown that increasing the grinding time enhances the magnetic properties while causing only minor changes in permittivity [34, 44].

The aim of this study was to develop a $BaTiO_3/BaFe_{12}O_{19}$ multiferroic composite with desirable magnetic and electrical properties. To achieve this, cost-effective processing route was used that involved ball milling of a powder mixture consisting of 20.0 wt% Fe and 80.0 wt% $BaTiO_3$, followed by sintering of the obtained ground samples. Ball milling produces fine particles with a large specific surface area and a high density of dislocations on the surface. By varying the grinding time, the morphology and microstructure of the sintered composites can be tailored, allowing for optimization of their functional properties for specific applications. The present work investigates the influence of the grinding time of 20.0 wt% Fe-80.0 wt% $BaTiO_3$ powder mixtures on the morphology, chemical composition, microstructure, as well as magnetic and electric properties of the sintered composites. The primary objective was to determine processing conditions that would allow the production of multiferroic composites with optimized magnetic and electrical performance.

2. Experimental

$BaTiO_3$ powder (Aldrich, St. Louis, MO, p.a. 99 wt%) was dispersed in 2-propanol and ball milled in air for 20 min using a planetary ball mill (Retsch PM 400). A powder mixture slurry consisting of 20.0 wt% Fe (Aldrich, St. Louis, MO, p.a. 99.99) and 80.0 wt% BaTiO3 was

then ball milled for periods ranging from 20 to 220 min. Disc-shaped samples (8.0 mm in diameter and 1.5 mm in thickness) were prepared by uniaxial pressing of the milled powder mixture at a pressure of 500 MPa. The samples were heated at a rate of 10 °C min^{-1} and sintered isothermally at 1200 °C for 2 h. Phase analysis was performed by X-ray diffraction (XRD) using a Bruker DM X-ray diffractometer operating in Bragg-Brentano geometry with $CuK_{\alpha,1}$ radiation ($\lambda_{K\alpha,1}$ = 0.15406 nm) at a grazing incidence angle of 0.5 deg. Diffraction patterns were recorded over the scattering angle 2θ from 10 to 90 deg with a step of 0.05 deg. The morphology, particle and aggregate size, and microstructure were examined using a Scanning Electron Microscope (SEM, JSM-6390 LV JEOL., 30kV) coupled with EDS and a Leica Q500 MC automatic device for microstructural analysis. Magnetic properties were studied by a modified Faraday method based on the interaction of the sample with an inhomogeneous magnetic field. The magnetic force was measured under argon atmosphere with a sensitivity of 10^{-7} N. The electrical properties were studied using an HP4191A multifrequency LCR instrument over the frequency range from 100 Hz to 500 MHz. To verify the reproducibility of the results, samples corresponding to each grinding time were prepared independently in three batches under identical processing conditions, and all measurements were performed on three parallel samples. The relative deviation of the measured magnetization values did not exceed 3%, while the relative uncertainty of the dielectric permittivity measurements was below 5%. The reported values represent the arithmetic mean of the parallel measurements.

3. Results and discussion

The powder mixture containing 20.0 wt% Fe and 80.0 wt% $BaTiO_3$ was ball milled for different durations, ranging from 0 to 220 min. The grinding time substantially influences the morphology, microstructure and chemical composition of the ground powder mixture [16, 33, 34, 47]. The milled powders were subsequently sintered at 1200 °C for 2 h and the resulting samples were characterized by SEM. The SEM micrographs revealed that the samples prepared from the powder mixture ground for 20-120 min consisted predominantly of plates with the size ranging from approximately 0.3 to 1.3 μm. For grinding times longer than 120 min, the microstructure was characterized by larger plates with sizes between 1.3 and 4.2 μm. In addition, prolonged grinding resulted in less distinct boundaries between plates, indicating an increased degree of particle coalescence during sintering. Particles of the sintered powders formed aggregates whose size increased with increasing grinding time of the starting mixture.

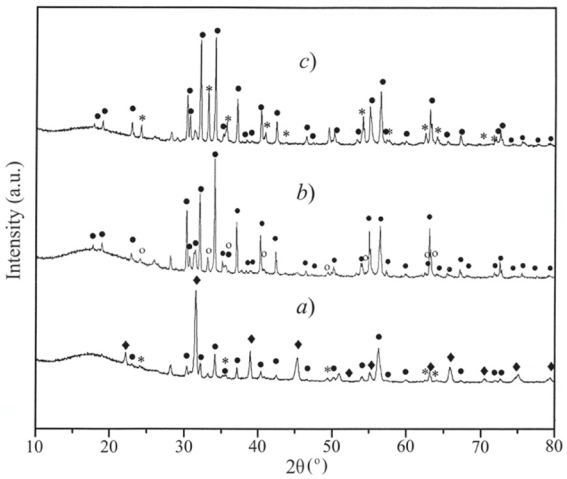

Fig. 1. XRD patterns of samples of sintered powder ground for *a*) 0 min; *b*) 90 min and *c*) 210 min. ● $BaFe_{12}O_{19}$; ♦ $BaTiO_3$;* $Ba_{1.696}Ti_{0.228}O_3$; ○ Fe_2O_3.

The phase composition of the sintered samples was determined by X-ray diffraction (XRD) Figure 1 presents XRD patterns of the sintered powders ground for 0, 90 and 210 min. The XRD pattern of the sintered sample prepared from the unmilled powder mixture exhibits intense diffraction peaks corresponding to $BaTiO_3$, weak peaks assigned to $BaFe_{12}O_{19}$ and barely detectable peaks of $Ba_{1.696}Ti_{0.228}O_3$. The low intensity peaks of $BaFe_{12}O_{19}$ indicate that only a portion of the Fe reacted, i.e. that a certain amount of Fe remained unreacted.

The reaction remains incomplete since the Fe particles are relatively large (approximately 1.5 μm) [16]. Consequently, the contact area between Fe and $BaTiO_3$ particles is limited, leading to slow formation of $BaFe_{12}O_{19}$. Prior to sintering, the ball-milled powder mixture containing 20.0 wt% Fe and 80.0 wt% $BaTiO_3$ consists of a $BaTiO_3$ matrix with embedded composite particles comprising a Fe core surrounded by a $BaTiO_3$ shell [16]. The $BaTiO_3$-coated particles, with an average size of 5.5 μm, effectively mask the diffraction signal from the Fe core, making the diffraction peaks of unreacted Fe difficult to detect in the XRD patterns [16, 33]. During sintering, $BaFe_{12}O_{19}$ and TiO_2 are formed as a result of a solid-state reaction (1) between the iron species and $BaTiO_3$:

$$12Fe + BaTiO_3 + 9O_2 \rightarrow \rightarrow BaFe_{12}O_{19} + TiO_2 \quad (1)$$

The TiO_2 produced in reaction (1) is amorphous and, therefore, does not show detectable peaks in the XRD patterns (Fig. 1). The weak peaks assigned to the $Ba_{1.696}Ti_{0.228}O_3$ phase are attributed to the reaction of a small fraction of $BaTiO_3$ with oxygen during sintering at elevated temperature, resulting in the formation of $Ba_{1.696}Ti_{0.228}O_3$ and amorphous TiO_2 according to Reaction (2):

$$1.696BaTiO_3 + 0.424O_2 = = Ba_{1.696}Ti_{0.228}O_3 + 1.468TiO_2 \quad (2)$$

Ball milling of the initial powder mixture results in fragmentation of both the powder particles and the crystal grains. In addition, the density of randomly distributed dislocations and inner microstrains increases, while the fraction of the crystalline $BaTiO_3$ and Fe phase decreases due to the formation of amorphous structures. Furthermore, as a result of the reaction of iron with atmospheric oxygen during the grinding of the initial powder mixture, partial oxidation of Fe to FeO, Fe_3O_4 and Fe_2O_3 occurs [16, 29, 33, 34]. With an increase in the milling time from 20 to 90 min, the intensity of the diffraction peaks of $BaTiO_3$ gradually decreases in the X-ray diffraction patterns of the sintered samples, while the intensity of the peaks of $BaFe_{12}O_{19}$ increases. These findings indicate that the fragmentation of $BaTiO_3$ and Fe particles promotes the formation of $BaFe_{12}O_{19}$ (reaction (1)) as a result of the increased contact area between the reactants, the higher density of dislocations and internal microstrains arising during the milling process. For milling times exceeding 90 min, crystalline $BaTiO_3$ undergoes almost complete transformation into the amorphous state as a consequence of the mechanical energy introduced by grinding [16]. As shown in the XRD pattern in Fig. 1, the residual unreacted $BaTiO_3$ (reaction (1)) remains predominantly in the amorphous state even after sintering and, therefore, does not produce detectable diffraction peaks. Weak peaks corresponding to Fe_2O_3 indicate oxidation of a fraction of Fe with atmospheric oxygen during sintering. In contrast, the XRD pattern of the sintered sample prepared from the powder ground for 210 min exhibits intense diffraction peaks of $BaFe_{12}O_{19}$ together with weak peaks of $Ba_{1.696}Ti_{0.228}O_3$. The absence of peaks corresponding to Fe oxides in Fig. 1c suggests that the iron oxides formed during grinding and sintering (FeO, Fe_3O_4 and Fe_2O_3) reacted completely with $BaTiO_3$, yielding $BaFe_{12}O_{19}$ and amorphous TiO_2, as described by Reactions (3)-(5):

$$24FeO + 6O_2 + 2BaTiO_3 \rightarrow \rightarrow 2BaFe_{12}O_{19} + 2TiO_2 \quad (3)$$

$$8Fe_3O_4 + 2O_2 + 2BaTiO_3 \rightarrow \rightarrow 2BaFe_{12}O_{19} + 2TiO_2 \quad (4)$$

$$12Fe_2O_3 + 2BaTiO_3 \rightarrow \rightarrow 2BaFe_{12}O_{19} + 2TiO_2 \quad (5)$$

XRD patterns of similar phase composition were obtained for the sintered samples prepared from the powders ground for 150 to 220 min.

As demonstrated by the above results, the sintered samples prepared from the powder mixture of 20.0 wt% Fe and 80.0 wt% $BaTiO_3$ after grinding for more than 90 min consist predominantly of an amorphous matrix composed of $BaTiO_3$ and TiO_2, inside which crystalline $BaFe_{12}O_{19}$ particles are embedded. The matrix also contains a negligible amount of $Ba_{1.696}Ti_{0.228}O_3$ crystallites.

The magnetic and electric properties of the sintered samples prepared from ground powder mixture consisting of 20.0 wt% Fe and 80.0 wt% $BaTiO_3$ strongly depend on the grinding time of the starting powder mixture. This dependence arises because the grinding process modifies the microstructure of the sintered sample, which in turn governs its magnetic and electric properties [33, 34]. Fig. 2 shows the variations of the magnetization of the sintered samples as a function of the grinding time of the starting powder mixture.

The magnetization of the freshly prepared sintered samples was determined 10 min after the application of the external magnetic field. As shown in Fig. 2, with the increase of grinding time from 0 to 90 min, the magnetization increased from 2.1 to 2.8 Am^2kg^{-1}. Further enhancement of the grinding time to 220 min resulted in a decrease in magnetization to 2.45 Am^2kg^{-1}. The increase in magnetization observed for grinding times less than 90 min can be attributed primarily to the enhanced formation of $BaFe_{12}O_{19}$ during sintering. Short grinding times produce relatively large particles of the starting powders, which exhibit lower reactivity and therefore slower reaction during sintering. Consequently, reactions (3) and (5) proceed incompletely, leading to a higher fraction of unreacted oxides FeO and α-Fe_2O_3.

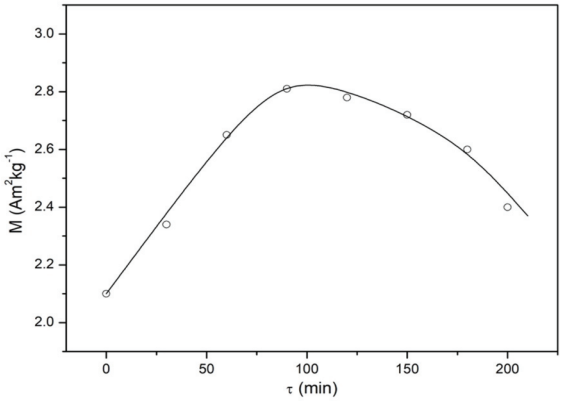

Fig. 2. Magnetization M of the sintered samples as a function of the grinding time (τ) of the starting powder mixture, measured at 22 °C.

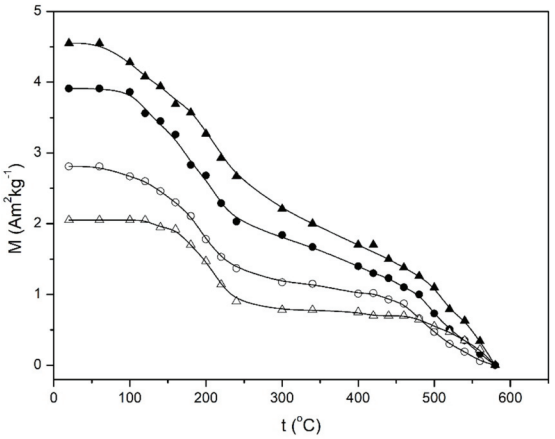

Fig. 3. Magnetization of sintered powders ground for 90 min (○, ●) and 210 min (△, ▲). Open symbols (○, △) represent the first heating cycle in the magnetic field. Filled symbols (●, ▲) correspond to the second cooling cycle in the magnetic field following the first cooling in the absence and the second heating in the presence of the magnetic field. Strength of the external magnetic field was 50kAm^{-1}. The heating and cooling rate was 10 °Cmin^{-1}.

The highest magnetization was obtained for sintered powders ground for approximately 90 minutes, suggesting that $BaFe_{12}O_{19}$ particles with the optimal average particle size were obtained in this regime. In contrast, prolonged grinding (90-220 min) promotes generation of larger particles of $BaFe_{12}O_{19}$ during sintering and a corresponding decrease in magnetization [50-52]. The measured magnetization values (2.1-2.8 Am^2kg^{-1} at an applied magnetic field of 50 kAm^{-1}) are comparable to those reported for sintered Fe-$BaTiO_3$ composites of similar composition and thermal history [16, 29, 33, 34]. In these materials, the magnetization is also governed by both the amount of $BaFe_{12}O_{19}$ particles formed and their mean size.

The effect of temperature on the magnetization of the sintered sample was also examined (Fig. 3). During the initial heating stage, from room temperature to 100 °C, the magnetization remained constant with no substantial fluctuations. A further increase in temperature from 100 to 250 °C resulted in a rapid decrease in magnetization. Between 250 to 470 °C, the magnetization exhibited only minor changes and remained nearly constant. In the temperature range from 470 °C to Curie temperature (570 °C) the magnetization decreased.

The presence of two distinct magnetization curves in Fig. 3 indicates the existence of two types of magnetic domains: a thermally stable domain and thermally less stable one. After the first heating cycle to 570 °C, the samples were cooled to 22 °C in the absence of an external magnetic field. They were then reheated to 570 °C in the presence of the magnetic field. The temperature dependence of the magnetization during the second heating was very similar to that observed during the first heating. In contrast, the second cooling cycle in the magnetic field resulted in significantly higher magnetization over the entire temperature range compared to the values measured during the first and second heating. This discrepancy is undoubtedly caused by the external magnetic field. In the directed $BaFe_{12}O_{19}$ domains, Fe^{3+} ions occupy five crystallographic sites: three octahedral sites 12k (spin-up), 2a (spin-up), and $4f_2$ (spin-down), one tetrahedral $4f_1$ (spin-down) and one bipyramidal 2b (spin-up). The magnetic moment of $BaFe_{12}O_{19}$ is defined as the algebraic sum of ion magnetic moments in different positions. In the presence of an external magnetic field, the Gibbs energy for spin-up sites decreases, whereas the Gibbs energy for spin-down centers increases by an amount corresponding to the magnetic energy of the Fe^{3+} ions in these states [45]. Since the domain contains more spin up than spin down sites, the total Gibbs energy of magnetic domains decreases with increasing magnetic field strength. Consequently, unfavorably oriented particles gradually become aligned under the influence of stronger external magnetic fields. Above the Curie temperature, both the domains and electron spins of the Fe^{3+} ions are randomly oriented. As a result of the sample cooling, the domains and spins of Fe^{3+} ions are oriented. All the above mentioned changes of spin up and spin down states result in the Gibbs activation energy decreasing for the process of transition of randomly oriented spins of 12k; 2a; 2b; $4f_1$ and

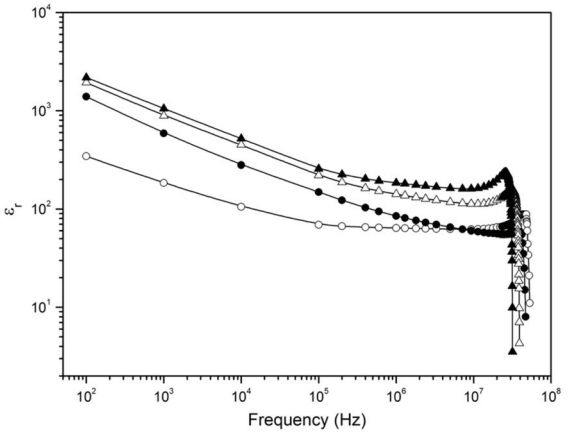

Fig. 4. Relative permittivity (ε_r) of sintered samples depending on the frequency (υ) of the applied electric field and the grinding time (τ) of the starting powder mixture containing 20.0 wt% Fe and 80.0 wt% $BaTiO_3$: ○ - 30 min; ● - 90 min; △- 180 min and ▲ - 210 min

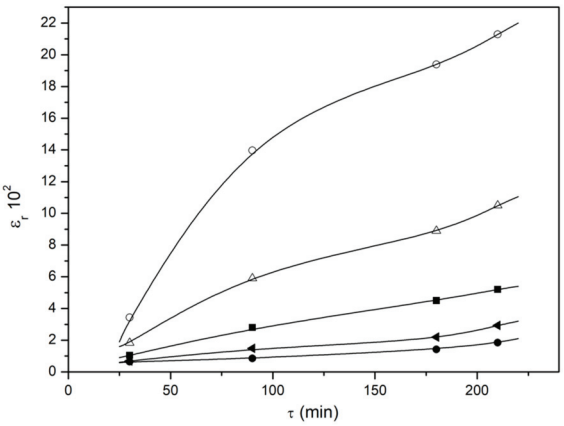

Fig. 5. Relative permittivity (ε_r) of sintered samples depending on the grinding time (τ) of the starting powder at different frequencies of the applied electric field: ○ - 100 Hz; △ - 10 kHz; ■ - 100 kHz; ◀ - 1.0 MHz and ● - 10 MHz.

$4f_2$ states into directed spin up states; while the Gibbs activation energy increasing for the process of transition of randomly oriented spins of $4f_1$ and $4f_2$ states into directed spin down states [45]. As a consequence, the formation of spin-up states is favored, whereas the formation of the spin-down states is suppressed by the external magnetic field. During sample cooling from temperatures above the Curie temperature to those lower than the Curie temperature in the external magnetic field, metastable spin-up $4f_1$ and $4f_2$ states are generated [45]. Since cooling of the sample to lower temperatures occurs relatively quickly, the process of transition of these metastable states $4f_1$ and $4f_2$ spin-up into the stable $4f_1$ and $4f_2$ spin-down states stops. Consequently, the sample cooled relatively rapidly in the external magnetic field exhibited a higher magnetization than that observed during the first heating cycle [45].

The electric properties of the sintered samples strongly depend on their chemical composition, microstructure and morphology. Fig. 4 shows the effect of the grinding time of the starting powder mixture (20.0 wt% Fe and 80.0 wt% $BaTiO_3$) and the frequency of the applied electric field on the relative dielectric permittivity of the sintered samples. The relative permittivity decreases with increasing frequency, whereas it rises when grinding time of the starting powder increases. The higher permittivity observed for sintered samples prepared from powders ground for longer times can be explained by the higher degree of amorphization of $BaTiO_3$. The amorphous $BaTiO_3$ phase is less ordered than its crystalline counterpart, allowing ions in higher energy states to move easily under the applied electric field and hence become polarized (Figs. 4 and 5). A similar decrease in relative permittivity with increasing frequency has been reported for barium hexaferrite ceramics and mechanically activated titanate ceramics [20, 30, 43]. This behavior is generally attributed to the reduced contribution of interfacial and dipolar polarization at higher frequencies.

The presented results demonstrate that the grinding time of the starting powder mixture substantially affects the phase composition, morphology and microstructure of the sintered composites, which in turn determine their magnetic and electric properties. Therefore, proper selection of the grinding time of the starting powder mixture provides an effective way to control the magnetic and dielectric properties of $BaTiO_3$-$BaFe_{12}O_{19}$ multiferroic composites for special applications.

4. Conclusion

The effect of grinding and subsequent sintering of a powder mixture containing 20.0 wt% Fe and 80.0 wt% $BaTiO_3$ on the morphology, chemical composition, microstructure, as well as magnetic and electric properties of the resulted samples was investigated. The sintered samples, prepared from the powders ground for 0 to 220 min consisted predominantly of plate-like shaped particles. Increasing the grinding time resulted in plate size growth from 0.3 to 4.2 μm, while the boundaries between them become progressively less distinct. The samples prepared from powders ground for less than 90 min consisted of a matrix containing crys-

talline $BaTiO_3$ together with the amorphous $BaTiO_3$ and TiO_2 phases, in which $BaFe_{12}O_{19}$ and $Ba_{1.696}Ti_{0.228}O_3$ crystallites were embedded. For grinding times longer than 90 min, the entire $BaTiO_3$ was in the amorphous state after sintering. The magnetization properties were strongly dependent on the grinding time. The magnetization of the sintered samples increased as the grinding time was extended up to 90 min, owing to enhanced formation of $BaFe_{12}O_{19}$ during the solid-state reactions involving FeO, α-Fe_2O_3 and $BaTiO_3$. Further increasing the grinding time led to a decrease in magnetization, which is attributed to changes in the microstructure, particularly formation of larger crystallites of $BaFe_{12}O_{19}$ during sintering. The temperature dependence of the magnetization revealed that the magnetization remained nearly constant up to 100 °C, decreased markedly between 100 to 250 °C, remained approximately constant in the temperature range of 250 to 470 °C, and decreased again on approaching the Curie temperature. Samples cooled from the Curie temperature in an applied magnetic field exhibited substantially higher magnetization than that obtained during the heating cycle. During cooling, $4f_1$ and $4f_2$ randomly distributed spins were transformed into metastable spin-up $4f_1$ and $4f_2$ states.

The dielectric properties were also affected by the grinding time. The relative permittivity rose with increasing grinding time of the starting powder mixture, whereas it decreased with increasing frequency of the external electric field. The enhanced permittivity of samples prepared from starting powders ground for longer times is attributed to reduced short-range order in the $BaTiO_3$ amorphous phase, which promotes the shift and polarization of ions under the action of the applied electric field.

Acknowledgments

This study was supported by the Ministry of Science, Technological Development and Innovation of the Republic of Serbia, Grant No. 451-03-66/2024-03/200132 University of Kragujevac, Faculty of Technical Sciences Čačak and Grant No. 451-03-66/2024-03/200288, University of Belgrade, Innovative Centre of the Faculty of Chemistry.

References

1. J. Aarts, Advances in materials science, Wiley-VCH, Weinheim, Vol. 5, 1993.
2. J.F. Scott, Multiferroic memories, Nat. Mater. 6 (2007).
3. C.-W. Nan, M.I. Bichurin, S. Dong, D. Viehland, G. Srinivasan, Multiferroic magnetoelectric composites: historical perspective, status, and future directions, J. Appl. Phys. 103 (2008) 031101. https://doi.org/10.1063/1.2836410.
4. K.F. Wang, J.-M. Liu, Z.F. Ren, Multiferroicity: the coupling between magnetic and polarization orders, Adv. Phys. 58 (2009) 321–448. https://doi.org/10.1080/00018730902920554.
5. R.C. Pullar, Hexagonal ferrites: a review of the synthesis, properties and applications of hexaferrite ceramics, Prog. Mater. Sci. 57 (2012) 1191–1334. https://doi.org/10.1016/j.pmatsci.2012.04.001.
6. J. Seidel, L.W. Martin, Q. He, Q. Zhan, Y.H. Chu, A. Rother, M.E. Hawkridge, P. Maksymovych, P. Yu, M. Gajek, N. Balke, S.V. Kalinin, S. Gemming, F. Wang, G. Catalan, J.F. Scott, N.A. Spaldin, J. Orenstein, R. Ramesh, Conduction at domain walls in oxide multiferroics, Nat. Mater. 8 (2009) 229–234.
7. M. Shandilya, R. Rai, K. Sharma, D. Thakur, Effect of addition of zinc ferrite on dielectric and magnetic properties of (Ba,Ca)TiO3 ceramics, Integr. Ferroelectr. 185 (2017) 147–154. https://doi.org/10.1080/10584587.2017.1370350.
8. M. Shandilya, R. Verma, Impedance modulated dielectric and magnetic properties of BCT-NF multiferroic composite, J. Magn. Magn. Mater. 527 (2021) 167782. https://doi.org/10.59277/RomJPhys.2025.70.615
9. Y. Yamasaki, S. Miyasaka, Y. Kaneko, J.-P. He, T. Arima, Y. Tokura, Magnetic reversal of the ferroelectric polarization in a multiferroic spinel oxide, Phys. Rev. Lett. 96 (2006) 207204. https://doi.org/10.1103/PhysRevLett.96.207204.
10. A. Haque, A.R. Mahbub, M. Abdullah-Al Mamun, M. Reaz, K. Ghosh, Fabrication and thickness-dependent magnetic studies of tunable multiferroic heterostructures (CFO/LSMO/LAO), Appl. Phys. A 125 (2019) 1–9. https://doi.org/10.1007/s00339-019-2620-y.
11. M. Radwan, M.M. Rashad, M.M. Hessien, Synthesis and characterization of barium hexaferrite nanoparticles, J. Mater. Process. Technol. 181 (2007) 106–109. https://doi.org/10.1016/j.jmatprotec.2006.03.015.
12. K. Martirosyan, E. Galstyan, S.M. Hossain, Y.-J. Wang, D. Litvinov, Barium hexaferrite nanoparticles: synthesis and magnetic properties, Mater. Sci. Eng. B 176 (2011) 8–13. https://doi.org/10.1016/j.mseb.2010.08.005.

13. V.V. Soman, V.M. Nanoti, D.K. Kulkarni, Dielectric and magnetic properties of Mg–Ti substituted barium hexaferrite, Ceram. Int. 39 (2013) 5713–5723. https://doi.org/10.1016/j.ceramint.2012.12.089.
14. P. Salcedo-Abraira, E. Morán, M.E. Villafuerte-Castrejón, R. Vivar-Ocampo, L. Pardo, Ba0.9Ca0.1TiO3: microwave-assisted hydrothermal synthesis and piezoelectric properties, Adv. Appl. Ceram. 117 (2018) 1–6. https://doi.org/10.1080/17436753.2017.1385991.
15. M. Reaz, A. Haque, K. Ghosh, Synthesis, characterization, and optimization of magnetoelectric BaTiO3–iron oxide core–shell nanoparticles, Nanomaterials 10 (2020) 563. https://doi.org/10.3390/nano10030563.
16. M. Spasojević Savković, M. Luković, M. Spasojević, A. Maričić, The effect of grinding and annealing temperature on microstructure and magnetic properties of the pressed powder mixture of 20.0 wt% Fe and 80.0 wt% BaTiO3, Rom. J. Phys. 71 (2025). https://doi.org/10.59277/RomJPhys.2025.70.615.
17. J.R. Mal, P. Hing, Sol-gel derived Ba(Fe,Ti)O3 ferroelectric materials for infrared sensors, J. Appl. Phys. 88 (2000) 1008–1014. https://doi.org/10.1063/1.373770.
18. H. Nakayama, H. Katayama-Yoshida, Theoretical prediction of magnetic properties of Ba(Ti1−xMx)O3 (M = Sc, V, Cr, Mn, Fe, Co, Ni, Cu), Jpn. J. Appl. Phys. 40 (2001) L1355–L1358. https://doi.org/10.1143/JJAP.40.L1355.
19. Z. Durmuş, A. Durmuş, H. Kavas, Synthesis and characterization of structural and magnetic properties of graphene/hard ferrite nanocomposites as microwave-absorbing material, J. Mater. Sci. 50 (2015) 1201–1213. https://doi.org/10.1007/s10853-014-8676-3.
20. J. Živojinović, D. Kosanović, V.A. Blagojević, V.P. Pavlović, N. Tadić, B. Vlahović, V.B. Pavlović, Dielectric properties of mechanically activated strontium titanate ceramics, Sci. Sinter. 54 (2022) 401–414. https://doi.org/10.2298/SOS2204401Z.
21. B. M. Ranđelović, S. Ribar, V.V. Mitić, B. Marković, H. Fecht, B. Vlahović, Artificial neural network applied on sintered BaTiO3 ceramic density, Sci. Sinter. 54 (2022) 425–438. https://doi.org/10.2298/SOS2204425R.
22. S. Filipović, N. Obradović, Lj. Anđelković, D. Olćan, J. Petrović, M. Mitrović, V. Pavlović, D. Jeremić, B. Vlahović, A. Đorđević, Multiferroic heterostructure BaTiO3/ε-Fe2O3 composite obtained by in situ reaction, Sci. Sinter. 53 (2021) 1–8. https://doi.org/10.2298/SOS2101001F.
23. V. Paunović, Z. Prijić, V.V. Mitić, Effect of donor and acceptor dopants on the microstructure and dielectric properties of barium titanate based ceramics, Sci. Sinter. 54 (2022) 81–91. https://doi.org/10.2298/SOS2201081P.
24. X. Gao, L. Li, J. Jiang, H. Wang, M. Fan, J. Huang, X. Wang, H. Wang, Vertically aligned nanocomposite BaTiO3:YMnO3 thin films with room temperature multiferroic properties toward nanoscale memory devices, ACS Appl. Nano Mater. 1 (2018) 2509–2514. https://doi.org/10.1021/acsanm.8b00614.
25. W. Zhang, M. Fan, L. Li, A. Chen, Q. Su, Q. Jia, J.L. MacManus-Driscoll, H. Wang, Heterointerface design and strain tuning in epitaxial BiFeO3:CoFe2O4 nanocomposite films, Appl. Phys. Lett. 107 (2015) 212901. https://doi.org/10.1063/1.4936157.
26. M. Fan, W. Zhang, J. Jian, J. Huang, H. Wang, Strong perpendicular exchange bias in epitaxial La0.7Sr0.3MnO3:LaFeO3 nanocomposite thin films, APL Mater. 4 (2016) 076105. https://doi.org/10.1063/1.4958965.
27. W.R. Zhang, A.P. Chen, J. Jian, Y.Y. Zhu, L. Chen, P. Lu, Q.X. Jia, J.L. MacManus-Driscoll, X.H. Zhang, H.Y. Wang, Strong perpendicular exchange bias in epitaxial La0.7Sr0.3MnO3: BiFeO3 nanocomposite films through vertical interfacial coupling, Nanoscale 7 (2015) 13808–13815. https://doi.org/10.1039/C5NR03231H.
28. B. Zhang, J. Huang, B.X. Rutherford, P. Lu, S. Misra, M. Kalaswad, Z. He, X. Gao, X. Sun, L. Li, H. Wang, Tunable, room-temperature multiferroic Fe–BaTiO3 vertically aligned nanocomposites with perpendicular magnetic anisotropy, Mater. Today Nano 11 (2020) 100083. https://doi.org/10.1016/j.mtnano.2020.100083.
29. M. Plazinić, M. Spasojević, M. Luković, A. Maričić, M. Spasojević, Effect of the mechanochemical activation, pressing and sintering of powders of 70% Fe and 30% BaTiO3 on morphology, microstructure, magnetic and electrical properties, J. Optoelectron. Adv. Mater. 23 (2021) 383–396.
30. D. Kosanović, V.A. Blagojević, A. Maričić, S. Aleksić, V.P. Pavlović, V.B. Pavlović, B. Vlahović, Influence of mechanical activation on functional properties of barium hexaferrite ceramics, Ceram. Int. 44 (2018) 6666–6672. https://doi.org/10.1016/j.ceramint.2018.01.078.
31. B. Zhang, M. Fan, L. Li, J. Jian, J. Huang, H. Wang, M. Kalaswad, H. Wang, Tunable magnetic anisotropy of self-assembled Fe nanostructures within a La0.5Sr0.5FeO3 matrix, Appl. Phys. Lett. 112 (2018) 013104. https://doi.org/10.1063/1.5008382.

32. S. Misra, L. Li, J. Jian, J. Huang, X. Wang, D. Zemlyanov, J.W. Jang, F.H. Ribeiro, H. Wang, Tailorable Au nanoparticles embedded in epitaxial TiO2 thin films for tunable optical properties, ACS Appl. Mater. Interfaces 10 (2018) 32895–32902.
33. O. Kosić, M. Luković, M. Spasojević-Savković, A. Maričić, M. Spasojević, Influence of grinding and pressing of the powder 50.0 wt% Fe, 47.0 wt% BaTiO3 and 3.0 wt% TiO2 on morphology, microstructure and magnetic properties, Sci. Sinter. 56 (2024) 381–383. https://doi.org/10.2298/SOS230706046K.
34. M. Luković, M. Spasojević-Savković, O. Kosić, T. Barudžija, A. Maričić, M. Spasojević, Influence of grinding, pressing and sintering of the powder 50.0 wt% Fe, 47.0 wt% BaTiO3 and 3.0 wt% TiO2 on morphology, microstructure, magnetic and electric properties, Sci. Sinter. 57 (2025) 1–18.
35. M. Dawber, K.M. Rabe, J.F. Scott, Physics of thin-film ferroelectric oxides, Rev. Mod. Phys. 77 (2005) 1083–1130. https://doi.org/10.1103/RevModPhys.77.1083.
36. V.N. Reddy, K.C. Babu Naidu, T. Subbarao, Structural, optical and ferroelectric properties of BaTiO3 ceramics, J. Ovonic Res. 12 (2016) 185–191.
37. T. Jin, L. Li, B. Zhang, H.Y.G. Lin, H. Wang, P.T. Lin, Monolithic mid-infrared integrated photonics using silicon-on-epitaxial barium titanate thin films, ACS Appl. Mater. Interfaces 9 (2017) 21848–21855. https://doi.org/10.1021/acsami.7b02681.
38. M.L. Schneider, C.A. Donnelly, S.E. Russek, B. Baek, M.R. Pufall, P.F. Hopkins, P.D. Dresselhaus, S.P. Benz, W.H. Rippard, Ultralow power artificial synapses using nanotextured magnetic Josephson junctions, Sci. Adv. 4 (2018) e1701329. https://doi.org/10.1126/sciadv.1701329.
39. R.M. Garcia, E.R. Ruiz, E.E. Rams, R.M. Sanchez, Effect of precursor milling on magnetic and structural properties of BaFe12O19 M-ferrite, J. Magn. Magn. Mater. 223 (2001) 133–137. https://doi.org/10.1016/S0304-8853(00)00599-0.
40. D.L. Sekulić, Z.Z. Lazarević, Č.D. Jovanović, A.N. Milutinović, N.Z. Romčević, Impedance spectroscopy of nanocrystalline MgFe2O4 and MnFe2O4 ferrite ceramics: effect of grain boundaries on the electrical properties, Sci. Sinter. 48 (2016) 17–28. https://doi.org/10.2298/SOS1601017S.
41. L. Junliang, Z. Yanwei, G. Cuijing, Z. Wei, Y. Xiaowei, One-step synthesis of barium hexaferrite nanopowders via microwave-assisted sol–gel auto-combustion, J. Eur. Ceram. Soc. 30 (2010) 993–997. https://doi.org/10.1016/j.jeurceramsoc.2009.10.019.
42. M.M. Rashad, M. Radwan, M.M. Hessien, Effect of Fe/Ba mole ratios and surface-active agents on the formation and magnetic properties of co-precipitated barium hexaferrite, J. Alloys Compd. 453 (2008) 304–308. https://doi.org/10.1016/j.jallcom.2006.11.080.
43. W.S. Castro, R.R. Corrêa, P.I.P. Filho, J.M.R. Mercury, A.A. Cabral, Dielectric and magnetic characterization of barium hexaferrite ceramics, Ceram. Int. 41 (2015) 241–246. https://doi.org/10.1016/j.ceramint.2014.08.064.
44. P. Shepherd, K.K. Mallick, R.J. Green, Magnetic and structural properties of M-type barium hexaferrite prepared by co-precipitation, J. Magn. Magn. Mater. 311 (2007) 683–692. https://doi.org/10.1016/j.jmmm.2006.08.046.
45. J. Smit, H.P.J. Wijn, Ferrites: Physical Properties of Ferrimagnetic Oxides in Relation to Their Technical Applications, Wiley, New York, 1959.
46. S. Rajan, P.M.M. Gazzali, G. Chandrasekaran, Electrical and magnetic phase transition studies of Fe and Mn co-doped BaTiO3, J. Alloys Compd. 656 (2016) 98–109. https://doi.org/10.1016/j.jallcom.2015.09.199.
47. A. Rani, J. Kolte, S.S. Vadla, P. Gopalan, Structural, electrical, magnetic and magnetoelectric properties of Fe doped BaTiO3 ceramics, Ceram. Int. 42 (2016) 8010–8016. https://doi.org/10.1016/j.ceramint.2016.01.205.
48. M. Spasojević-Savković, M. Luković, M. Spasojević, A. Maričić, Mathematical model of the effect of temperature and annealing time on magnetization of the alloy of BaFe12O19 nanocrystals and the amorphous phase of BaTiO3 and TiO2, Rom. J. Phys. 70 (2025) 1–19. https://doi.org/10.59277/RomJPhys.2025.70.603.
49. K. Samuvel, K. Ramachandran, Structure, electrical and magnetic property investigations on Fe-doped hexagonal BaTiO3, Optik 127 (2016) 1781–1786. https://doi.org/10.1016/j.ijleo.2015.10.240.
50. X. Zhang, Z. Yue, Y. Zhang, Structure characterization and magnetic properties of barium hexaferrite films deposited on 6H-SiC with random in-plane orientation, Ceram. Int. 43 (2017) 8611–8615. https://doi.org/10.1016/j.ceramint.2017.03.169.
51. F.M. Silva Júnior, C.W.A. Paschoal, Spin–phonon coupling in BaFe12O19 M-type hexaferrite, J. Appl. Phys. 116 (2014) 244110. https://doi.org/10.1063/1.4904062.

52. C. Suryanarayana, E. Ivanov, V.V. Boldyrev, The science and technology of mechanical alloying, Mater. Sci. Eng. A 304–306 (2001) 151–158. https://doi.org/10.1016/S0921-5093(00)01465-9.
53. M. Spasojević, N. Ćirović, L. Ribić-Zelenović, P. Spasojević, A. Maričić, Effect of deposition current density and annealing temperature on the microstructure, hardness and electrical and magnetic properties of electrodeposited Ni–Fe–W alloy, J. Electrochem. Soc. 161 (2014) D463. https://doi.org/10.1149/2.0041410jes.
54. R. Miličić, M. Spasojević, M. Spasojević, A. Maričić, S. Ranđić, Amorphous–crystalline Ni–Fe powder mixture: hydrogenation and annealing effects on microstructure and electrical and magnetic properties, Sci. Sinter. 48 (2016) 343–351. https://doi.org/10.2298/SOS1603343M.
55. L. Ribić-Zelenović, M. Spasojević, A. Maričić, M. Ristić, The effect of structural changes during sintering on the electric and magnetic traits of the Ni96.7Mo3.3 alloy nanostructured powder, Sci. Sinter. 41 (2009) 175–184. https://doi.org/10.2298/SOS0902175R.
56. M. Spasojević, L. Ribić-Zelenović, A. Maričić, M. Ristić, Nanostructured Ni–Fe–W alloy electrodeposits: mechanical and structural characteristics after heat-treatment, Sci. Sinter. 43 (2011) 313–327. https://doi.org/10.2298/SOS1103313S.